Linear models enable powerful differential activity analysis in massively parallel reporter assays

Leslie Myint[1], Dimitrios G. Avramopoulos[2], Loyal A. Goff[2,3], and Kasper D. Hansen[1,2,*]

[1]Department of Biostatistics, Johns Hopkins Bloomberg School of Public Health
[2]McKusick-Nathans Institute of Genetic Medicine, Johns Hopkins School of Medicine
[3]Department of Neuroscience, Johns Hopkins School of Medicine

Abstract

Massively parallel reporter assays (MPRAs) have emerged as a popular means for understanding noncoding variation in a variety of conditions. However, development of statistical analysis methods has not kept pace with the use of this assay. We present a linear model framework, mpralm, for the differential analysis of activity measures from these experiments that we show is calibrated and powerful. We show that it outperforms statistical tests that are commonly used in the literature. Further, we investigate theoretical and real-data properties of barcode summarization methods. These results inform recommendations for differential analysis, general group comparisons, and study design in terms of sample sizes and sequencing depth.

*To whom correspondence should be addressed. Email: khansen@jhsph.edu

Introduction

Noncoding regions in the human genome represent the overwhelming majority of genomic sequence, but their function remains largely uncharacterized. Better understanding of the functional consequences of these regions has the potential to greatly enrich our understanding of biology.

It is well understood that some noncoding regions are regulatory in nature. It has been straightforward to experimentally test the regulatory ability of a given DNA sequence with standard reporter assays, but these assays are low throughout and do not scale to the testing of large numbers of sequences. Massively parallel reporter assays (MPRA) have emerged as a high-throughput means of measuring the ability of sequences to drive expression (White, 2015; Melnikov, Zhang, et al., 2014). These assays build on the traditional reporter assay framework by coupling each putative regulatory sequence with several short DNA tags, or barcodes, that are incorporated into the RNA output. These tags are counted in the RNA reads and the input DNA, and the resulting counts are used to quantify the activity of a given putative regulatory sequence, typically involving the ratio of RNA counts to DNA counts (Figure 1).

The applications of MPRA have been diverse, and there have been correspondingly diverse methods used in statistical analysis. There are three broad categories of MPRA applications: characterization studies, saturation mutagenesis, and differential analysis.

Characterization studies examine thousands of different putative regulatory elements that have a wide variety of sequence features and try to correlate these sequence features with measured activity levels (Grossman et al., 2017; Guo et al., 2017; Safra et al., 2017; Levo et al., 2017; Maricque, Dougherty, and Cohen, 2017; Groff et al., 2016; Ernst et al., 2016; White, Kwasnieski, et al., 2016; Ferreira et al., 2016; Fiore and Cohen, 2016; Farley et al., 2015; Kamps-Hughes et al., 2015; Dickel et al., 2014; Kwasnieski, Fiore, et al., 2014; Mogno, Kwasnieski, and Cohen, 2013; Gisselbrecht et al., 2013; White, Myers, et al., 2013; Smith et al., 2013). Typical statistical analyses use regression to study the impact of multiple features simultaneously. They also compare continuous activity measures or categorized (high/low) activity measures across groups using paired and unpaired t-, rank, Fisher's exact, and chi-squared tests.

Saturation mutagenesis studies look at only a few established enhancers and examine the impact on activity of every possible mutation at each base as well as interactions between these mutations (Patwardhan, Lee, et al., 2009; Melnikov, Murugan, et al., 2012; Patwardhan, Hiatt, et al., 2012; Kwasnieski, Mogno, et al., 2012; Kheradpour et al., 2013; Birnbaum et al., 2014; Zhao et al., 2014). Analyses have uniformly used linear regression where each position in the enhancer sequence is a predictor.

Differential analysis studies look at thousands of different elements, each of which has two or more versions. Versions can correspond to allelic versions of a sequence (Ulirsch et al., 2016; Tewhey et al., 2016; Vockley et al., 2015) or different environmental contexts

(Inoue et al., 2017), such as different cell or tissue types (Shen et al., 2016). These studies have compared different sequences versions using paired t-tests, rank sum tests, and Fisher's exact test (by pooling counts over biological replicates).

Despite the increasing popularity of this assay, guiding principles for statistical analysis have not been put forth. Researchers still use a large variety of ad hoc methods for analysis. For example, there has been considerable diversity in the earlier stages of summarization of information over barcodes. Barcodes are viewed as technical replicates of the regulatory element sequences, and groups have considered numerous methods for summarizing barcode-level information into one activity measure per enhancer. On top of this, a large variety of statistical tests are used to make comparisons.

Because counts from sequencing technologies are the main source of data in these experiments, it is natural to think about standard discrete models for count data. However, careful consideration is warranted because the quantities of interest are not the counts themselves but rather ratios of counts (RNA/DNA) or some form of input (DNA)-adjusted counts of output (RNA). Note that both RNA and DNA readouts are stochastic in nature. Recently, a method called QuASAR-MPRA was developed to identify regulatory sequences that have allele-specific activity (Kalita et al., 2017). This method uses a beta-binomial model to model RNA counts as a function of DNA counts, and it provides a means for identifying sequences that show a significant difference in regulatory activity between two alleles. While it provides a framework for two group comparisons within MPRAs, QuASAR-MPRA is limited in this regard because experiments might have several conditions and involve arbitrary comparisons.

To our knowledge, no method has been developed that provides tools for general purpose differential analysis of activity measures from MPRA. General purpose methods are ones that can flexibly analyze data from a range of study designs. While it is often of interest to study the effect of sequence features on the estimated activity levels of MPRA sequences (using tools such as MPAthic (Ireland and Kinney, 2016)), typically some sort of differential analysis is needed first to group interesting sequences together. This would usually involve comparing the activity of each putative regulatory sequence of interest to a suitable negative control.

We present mpralm, a method for testing for differential activity in MPRA experiments. Our method uses linear models as opposed to count-based models to identify differential activity. This approach provides desired analytic flexibility for more complicated experimental designs that necessitate more complex models. It also builds on an established method that has a solid theoretical and computational framework (Law et al., 2014). We show that mpralm can be applied to a wide variety of MPRA datasets and has good statistical properties related to type I error control and power. Furthermore, we examine proper techniques for combining information over barcodes and provide guidelines for choosing sample sizes and sequencing depth when considering power. Our method is open source and freely available in the *mpra* package for R on the Bioconductor reposi-

tory: https://bioconductor.org/packages/mpra.

Results

The structure of MPRA data and experiments

MPRA data consists of measuring the activity of some putative regulatory sequences, henceforth referred to as "elements". First a plasmid library of oligos is constructed, where each element is coupled with a number of short DNA tags or barcodes. This plasmid library is then transfected into one or more cellular contexts, either as free-floating plasmids or integrated into the genome (Inoue et al., 2017). Next, RNA output is measured using RNA sequencing, and DNA output as a proxy for element copy number is measured using DNA sequencing (occasionally, element copy number is unmeasured), giving the data structure shown in Figure 1. The log-ratio of RNA to DNA counts is commonly used as an activity outcome measure.

Since each element is measured across a number of barcodes, one needs to summarize this data into a single activity measure a for a single element in a single sample. Multiple approaches have been proposed for this summarization step. We consider two approaches. First is averaging, where a log-ratio is computed for each barcode, then averaged across barcodes. This treats the different barcodes as technical replicates. The second approach is aggregation, where RNA and DNA counts are each summed across barcodes, followed by formation of a log-ratio. This approach effectively uses the barcodes to simply increase the sequencing counts for that element.

In our investigation of the characteristics of MPRA data we use a number of datasets listed in Table 1 (Methods). We have divided them into 3 categories. Two of the categories are focused on differential analysis: one category on comparing different alleles and one category on comparing the same element in different conditions (retina vs. cortex and episomal vs. chromosomal integration). The two allelic studies naturally involve paired comparisons in that the two elements being compared are always measured together in a single sample (which is replicated). Finally, we are using two different saturation mutagenesis experiments.

The variability of MPRA data depends on element copy number

It is well established that count data from RNA sequencing studies exhibit a mean-variance relationship (McCarthy, Chen, and Smyth, 2012). On the log scale, low counts are more variable across replicates than high counts, at least partly due to inherent Poisson variation in the sequencing process (Marioni et al., 2008; Bullard et al., 2010). This relationship has been leveraged in both count-based analysis methods (Robinson, McCarthy,

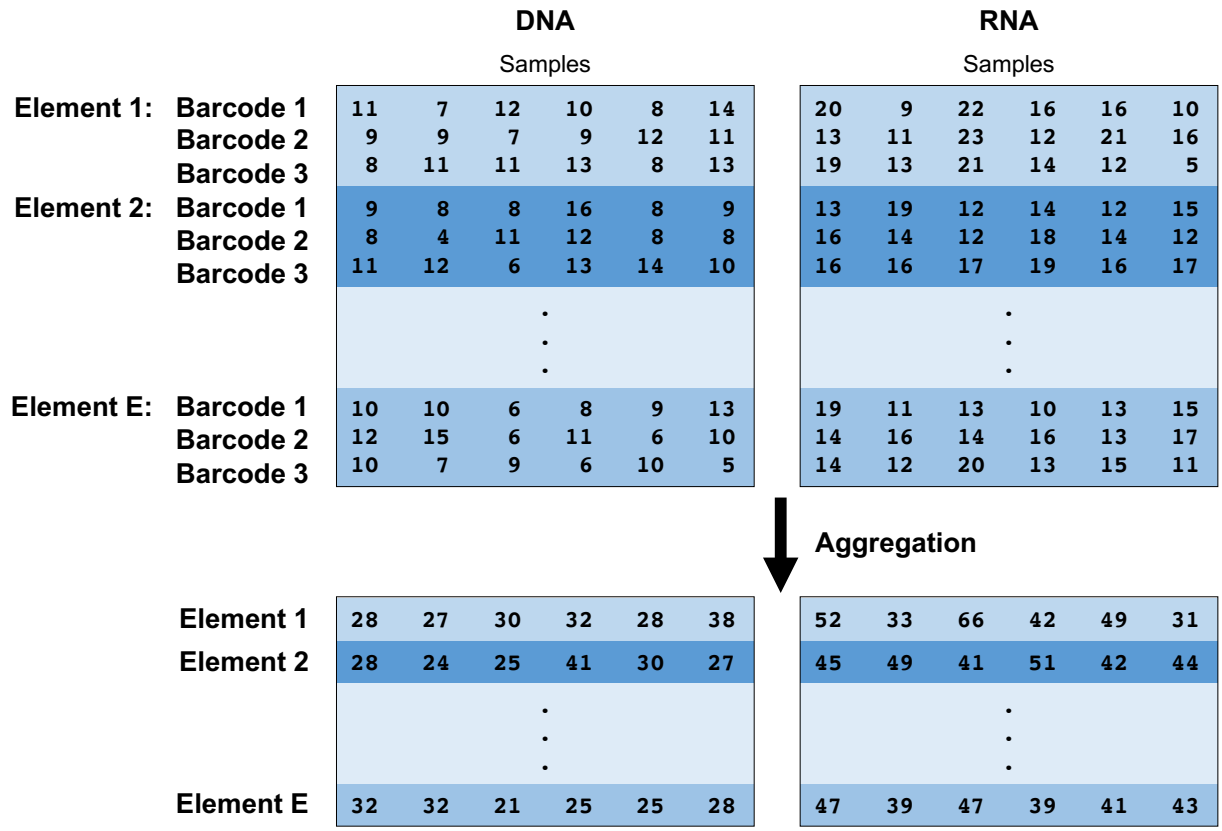

Figure 1. Structure of MPRA data. Thousands of putative regulatory elements can be assayed at a time in an MPRA experiment. Each element is linked to multiple barcodes. A plasmid library containing these barcoded elements is transfected into several cell populations (samples). Cellular DNA and RNA can be isolated and sequenced. The barcodes associated with each putative regulatory element can be counted to obtain relative abundances of each element in DNA and RNA. The process of aggregation sums counts over barcodes for element in each sample. Aggregation is one method for summarizing barcode level data into element level data.

and Smyth, 2010; Love, Huber, and Anders, 2014) and more recently linear model-based methods (Law et al., 2014) to, respectively, improve dispersion estimates and to estimate weights reflecting inherent differences in variability for count observations from different samples and genes.

Because MPRAs are fundamentally sequencing assays, it is useful to know whether similar variance relationships hold in these experiments. Due to the construction of MPRA measurements, each element is present in a different (random) copy number, and this copy number ought to impact both background and signal measurements from the el-

Table 1. Datasets

Dataset	Description	Cell culture	Replicates	Barcodes
Differential analysis: alleles				
Tewhey	Study of 39,479 oligos coming from 29,173 variants to follow up on prior eQTL results. Large initial oligo pool: 79k. Second pool: 7.5k.	NA12878 (LCL) NA19239 (LCL) HepG2	NA12878: 5 NA19239: 3 HepG2: 5	79k pool: ∼73 7.5k pool: ∼350
Ulirsch	Study of 2756 variants in strong LD with 75 main variants to identify loci that affect RBC traits.	K562, K562 with GATA1 over-expr.	K562: 6 K562+GATA1: 4	14
Differential analysis: conditions				
Inoue	Comparison of episomal and lentiviral MPRA.	HepG2	3	Max: 99.
Shen	Study of tissue specificity of cis-regulatory elements in-vivo in mouse.	Mouse retina and cerebral cortex	3	∼8
Saturation mutagenesis				
Melnikov	Two inducible enhancers: (1) a synthetic cAMP-regulated enhancer and (2) the virus-inducible interferon-beta enhancer. Single-hit scanning alters one base at a time. Multi-hit sampling alters several bases at a time.	HEK293T	Single: 2 Multi: 2	Single: 13 Multi: 1
Kheradpour	Study of 2104 wild-type sequences and 3314 variant sequences containing targeted motif disruptions to understand base-level effects in motifs.	K562, HepG2	2	10

ement. We are therefore specifically interested in the functional relationship between element copy number and the variability of the activity outcome measure. As outcome measure we use the log-ratio of RNA counts to DNA counts (aggregate estimator), and we use aggregated DNA counts, averaged across samples, as an estimate of DNA copy number. We compute empirical standard deviations of the library size-corrected outcome measure across samples. In Figure 2 we depict this relationship across the previously discussed publicly available datasets (Table 1). For all datasets, with one exception, there is higher variation associated with lower copy number. The functional form is reminiscent of the mean-variance relationship in RNA sequencing data (Law et al., 2014), despite that we here show variance of a log-ratio of sequencing counts.

Statistical modeling of MPRA data

To model MPRA data we propose to use a simple variant of the voom methodology (Law et al., 2014), proposed for analysis of RNA sequencing data. This methodology is based on standard linear models, which are coupled with inverse variance weights representing the mean-variance relationship inherent in RNA sequencing data. The weights are derived from smoothing an empirical mean-variance plot. Similar to voom, we propose to use linear models to model log-ratio MPRA data, but we estimate weights by smoothing the relationship between empirical variance of the log-ratios and log-DNA copy number, as depicted in Figure 2. This approach has a number of advantages. (1) It is flexible to different functional forms of the variance-copy number relationship. (2) It allows for a unified approach to modeling many different types of MPRA design using the power of design matrices. (3) It allows for borrowing of information across elements using empir-

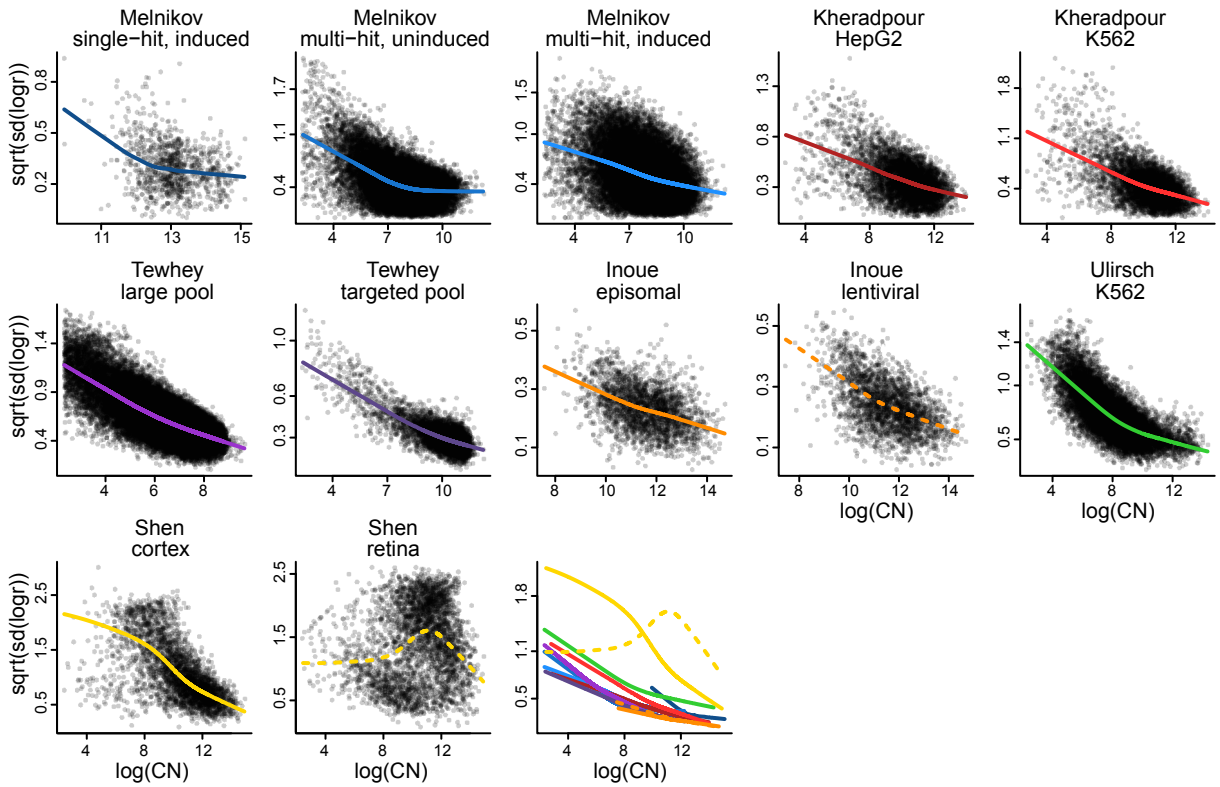

Figure 2. Variability of MPRA activity measures depends on element copy number. For multiple publicly available datasets we compute activity measures of putative regulatory element as the log2 ratio of aggregated RNA counts over aggregated DNA counts. Each panel shows the relationship between variability (across samples) of these activity measures and the average log2 DNA levels (across samples). Depicted is a lowess curve representing the local average variability. The last plot depicts all lowess curves on the same figure.

ical Bayes techniques. (4) It allows for different levels of correlation between elements using random effects. We call this approach mpralm.

The current literature on analysis of MPRA experiments contains many variant methods (see Introduction). To evaluate mpralm, we compare the method to the following variants used in the literature: QuASAR-MPRA, t-tests, and Fisher's exact test. QuASAR-MPRA is a recently developed method that is targeted for the differential analysis of MPRA data (Kalita et al., 2017). It specifically addresses a two group differential analysis where the two groups are elements with two alleles and uses base-calling error rate in the model formulation. It collapses count information across samples to create three pieces of information for each element: one count for RNA reads for the reference allele, one count for RNA reads for the alternate allele, and one proportion that gives the fraction of DNA reads corresponding to the reference allele. Fisher's exact test similarly collapses count information across samples. To test for differential activity, a 2-by-G table is formed with

RNA and DNA designation forming one dimension and condition designation (with G groups) in the second dimension. The t-test operates on the log ratio outcomes directly; we use the aggregate estimator to summarize over barcodes. Either a paired or unpaired t-test is used based on experimental design.

Studies comparing different alleles (Tewhey et al., 2016; Ulirsch et al., 2016), are naturally paired in the sense that both alleles are measured at the same time in the same sample. We can model that using mpralm by using a random effect representing the loci. Similarly, this can be incorporated into t-tests by using paired t-tests. Note that the random effect approach immediately generalizes to settings where more than two alleles are compared, unlike both paired t-tests and QuASAR-MPRA.

mpralm is a powerful and well-calibrated method for differential analysis

First, we focus on evaluating the performance of mpralm for differential analysis. We compare to QuASAR-MPRA, t-tests, and Fisher's exact test. We use four of the previously discussed studies, specifically the Tewhey, Inoue, Ulirsch and Shen studies. Two of these studies (Tewhey, Ulirsch) focuses on comparing the activity of elements with two alleles, whereas the other two (Inoue, Shen) compare the activity of each element in two different conditions. For the allelic studies, we use a random effects model for mpralm and paired t-tests. Both Tewhey et al. (2016) and Ulirsch et al. (2016) compare alleles in different cellular contexts; we observe similar behavior of all evaluations in all contexts (data not shown) and have therefore chosen to depict results from one cellular context for both of these studies. For Tewhey et al. (2016) we depict results both from a large pool of elements used for initial screening and a smaller, targeted pool.

Figure 3 shows p-value distributions that result from running mpralm, QuASAR-MPRA, t-tests, and Fisher's exact test. Across these datasets, all methods except for QuASAR show a well-behaved p-value distribution; high p-values appear uniformly distributed, and there is a peak at low p-values. Fisher's exact test has a very high peak around zero. We examine mpralm using both an average estimator and an aggregation estimator for summarizing across barcodes; this cannot be done for the Tewey dataset where we do not have access to barcode-level data. We were unable to run QuASAR-MPRA for the Shen dataset. To fully interpret these p-value distributions, we need to assess error rates.

To estimate empirical type I error rates, we performed permutations. Specifically, we created curated null permutations where each permuted sample group was composed of half of the samples from group 1 and half of the samples from group 2. We performed up to 100 permutations, if sample size permitted. mpralm is built on limma which utilizes an empirical Bayes step to borrow strength across genes for estimating gene specific variances. It has recently been shown that permuting sample labels results in inaccurate estimates of error rates for limma, due to the empirical Bayes step, and that accurate error rates for a two-group comparison can be obtained by permuting residuals (Jiang,

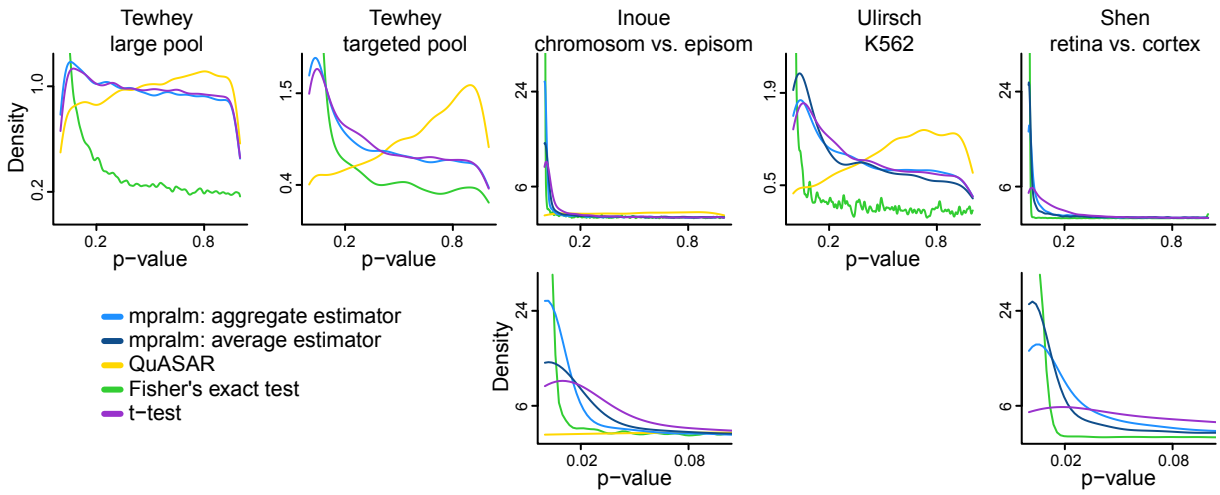

Figure 3. Comparison of detection rates and p-value calibration over datasets. The distribution of p-values for all datasets, including a zoom of the $[0, 0.1]$ interval for some datasets. Over all datasets, most methods show p-values that closely follow the classic mixture of uniformly distributed p-values with an enrichment of low p-values for differential elements. For the datasets which had barcode level counts (Inoue, Ulirsch, and Shen), we used two types of estimators of the activity measure (log ratio of RNA/DNA) with mpralm, shown in light and dark blue. We were not able to run QuASAR on the Shen mouse dataset.

2017). We utilize this procedure to estimate error rates for mpralm, and observe that this dramatically changes our error estimates (data not shown).

Figure 4 depicts estimated empirical type I error rates (estimated as the median error rate over the 100 permutations). We observe that Fisher's exact test has wildly inflated type I error, presumably because the data is overdispersed. mpralm is well calibrated, t-tests are conservative and QuASAR-MPRA less so.

To investigate the trade-off between observed power (number of rejected tests) and type I error rates, we combine these quantities in two ways. In Figure 5 we display the number of rejections as a function of observed type I error rates. In this display, we have essentially used the observed type I rate displayed in Figure 4 to calibrate the nominal alpha-level. For a fixed error rate, we interpret a high number of rejections to suggest high power. Both Fisher's exact test and QuASAR-MPRA show poor performance. T-tests are surprisingly competitive, especially for error rates greater than 0.1. If we know the proportion of true null hypotheses π_0, we can translate these rates into false discovery rates. This is an unknown quantity, but we estimate it using a method developed by Phipson (2013) and thereby compute an estimated false discovery rate. In Figure 6 the estimated false discovery rate (for a given π_0) is displayed as a function of the number of rejections. For the Tewhey study we see great performance for t-tests while mpralm is

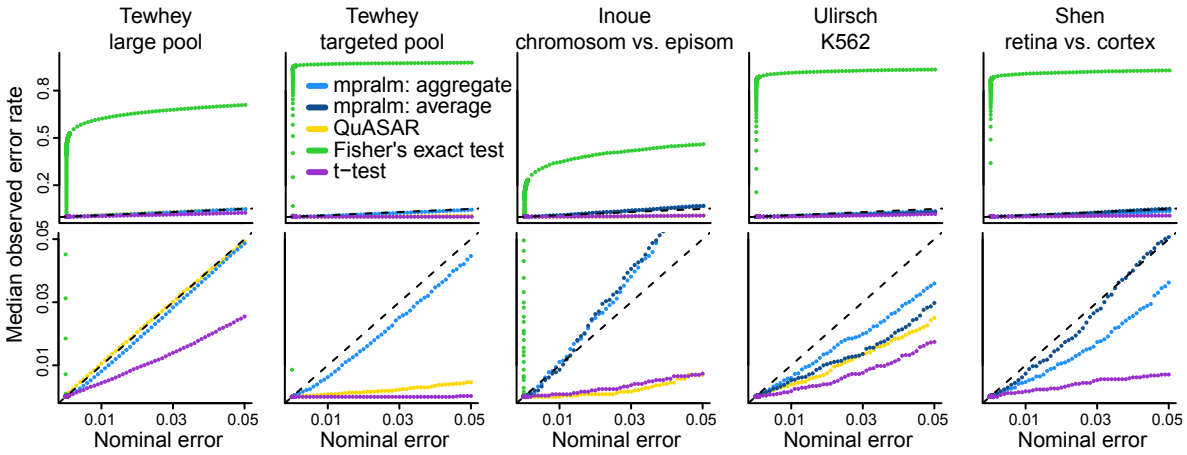

Figure 4. Empirical type I error rates. Type I error rates were estimated for all methods at different nominal levels with null permutation experiments (Methods). For the datasets which had barcode level counts (Inoue, Ulirsch, and Shen), we used two types of estimators of the activity measure (log ratio of RNA/DNA) with mpralm, shown in dark and light blue.

best for the Shen study.

In conclusion, we observe that Fisher's exact test has a high error rate and that QuASAR-MPRA is underpowered; based on these results we cannot recommend either method. mpralm and t-tests are both much better than these two tests. However, t-tests should only be used if the error rates are empirically calibrated as we have done here. mpralm works well without any calibration.

Comparison of element rankings between methods

The power and error evaluations discussed above, suggests that t-tests are competitive to mpralm, if type I error calibration is performed. While these are important metrics to consider when choosing an analysis method, it is also important to consider ranking quality in high-throughput studies. We observe fairly different rankings between mpralm and the t-test and examine drivers of these differences in Figure 7. For each dataset, we find the MPRA elements that appear in the top 200 elements with one method but not the other. We will call these uniquely top ranking elements, and they range from 24% to 64% depending on dataset. For these uniquely top ranking elements, we compute the mean log DNA, log RNA, and log-ratio measures and determine where these fall in the overall distributions of these quantities. These percentiles are compared between mpralm and the t-test in the first three rows of Figure 7. For most datasets, DNA, RNA, and log-ratio activity measures are higher in uniquely top ranking mpralm elements. It is desirable for top ranking elements to have higher values for all three quantities because higher DNA

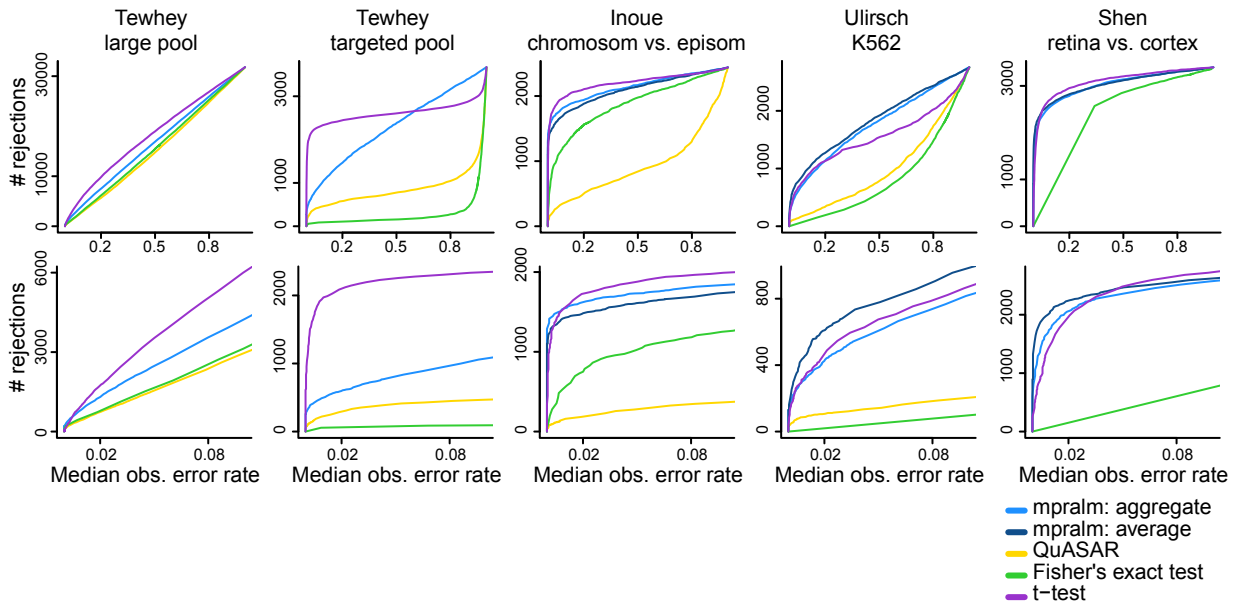

Figure 5. Number of rejections as a function of observed error rate. To compare the detection (rejection) rates of the methods fairly, we compare them at the same observed type I error rates, estimated in Figure 4. The bottom row is a zoomed-in version of the top row. We see that the t-test and mpralm consistently have much higher detection rates than Fisher's exact test and QuASAR. The t-test has high detection rates at higher error rates, and mpralm has higher detection rates at low error rates.

levels increase confidence in the activity measure estimation, and higher RNA and log-ratio values give a stronger indication that a particular MPRA element has regulatory activity.

In the last two rows of Figure 7, we compare effect sizes and variability measures (residual standard deviations). The t-test uniformly shows lower variability but also lower effect sizes for its uniquely top ranking elements. This follows experience from gene-expression studies where standard t-tests tends to underestimate the variance and thereby exhibit t-statistics which are too large, leading to false positives. In MPRA studies, as with most other high-throughput studies, it is typically more useful to have elements with high effect sizes at the top of the list. Such elements are able to picked out in mpralm due to its information sharing and weighting framework.

mpralm enables modeling for complex comparisons

While many comparisons of interest in MPRA studies can be posed as a two group comparison (e.g. major allele vs. minor allele), more complicated experimental designs are also of interest. For example, in the allelic study conducted by Ulirsch et al. (2016), puta-

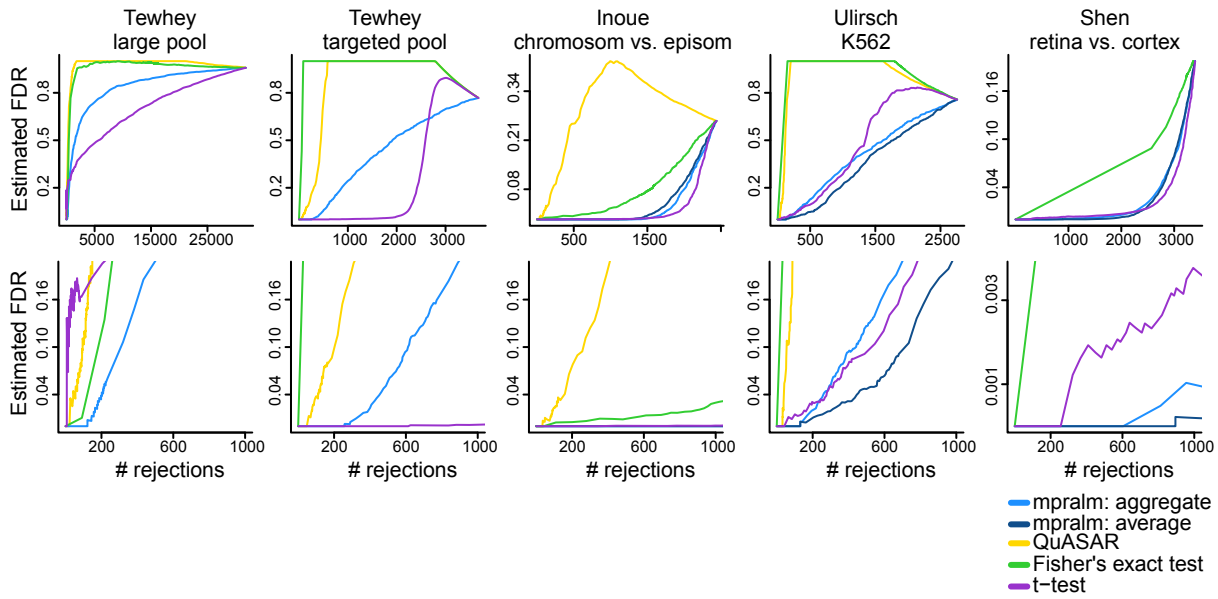

Figure 6. Estimated FDR. For each dataset and method, the false discovery rate is estimated as a function of the number of rejections. This requires estimation of the proportion of true null hypotheses (Methods). The bottom row is a zoomed-in version of the top row.

tive biallelic enhancer sequences are compared in two cellular contexts. The first is a standard culture of K562 cells, and the second is a K562 culture that induces over-expression of GATA1 for a more terminally-differentiated phenotype. A straightforward question is whether an allele's effect on enhancer activity differs between cellular contexts. Let y_{eia} be the enhancer activity measure (log ratio of RNA over DNA counts) for element e, in sample i for allele a. Let x_{1eia} be a binary indicator of the mutant allele. Let x_{2eia} be a binary indicator of the GATA1 over-expression condition. Then the following model

$$Y_{eia} = \beta_{0e} + \beta_{1e}x_{1eia} + \beta_{2e}x_{2eia} + \beta_{3e}x_{1eia}x_{2eia} + b_i + \epsilon_{eia}$$

is a linear mixed effects model for activity measures, where b_i is a random effect that induces correlation between the two alleles measured within the same sample. We can perform inference on the β_{3e} parameters to determine differential allelic effects. Such a model is easy to fit within the mpralm framework, since our framework supports model specifications by general design matrices. In contrast, this question cannot be formulated in the QuASAR, t-test, and Fisher's exact test frameworks.

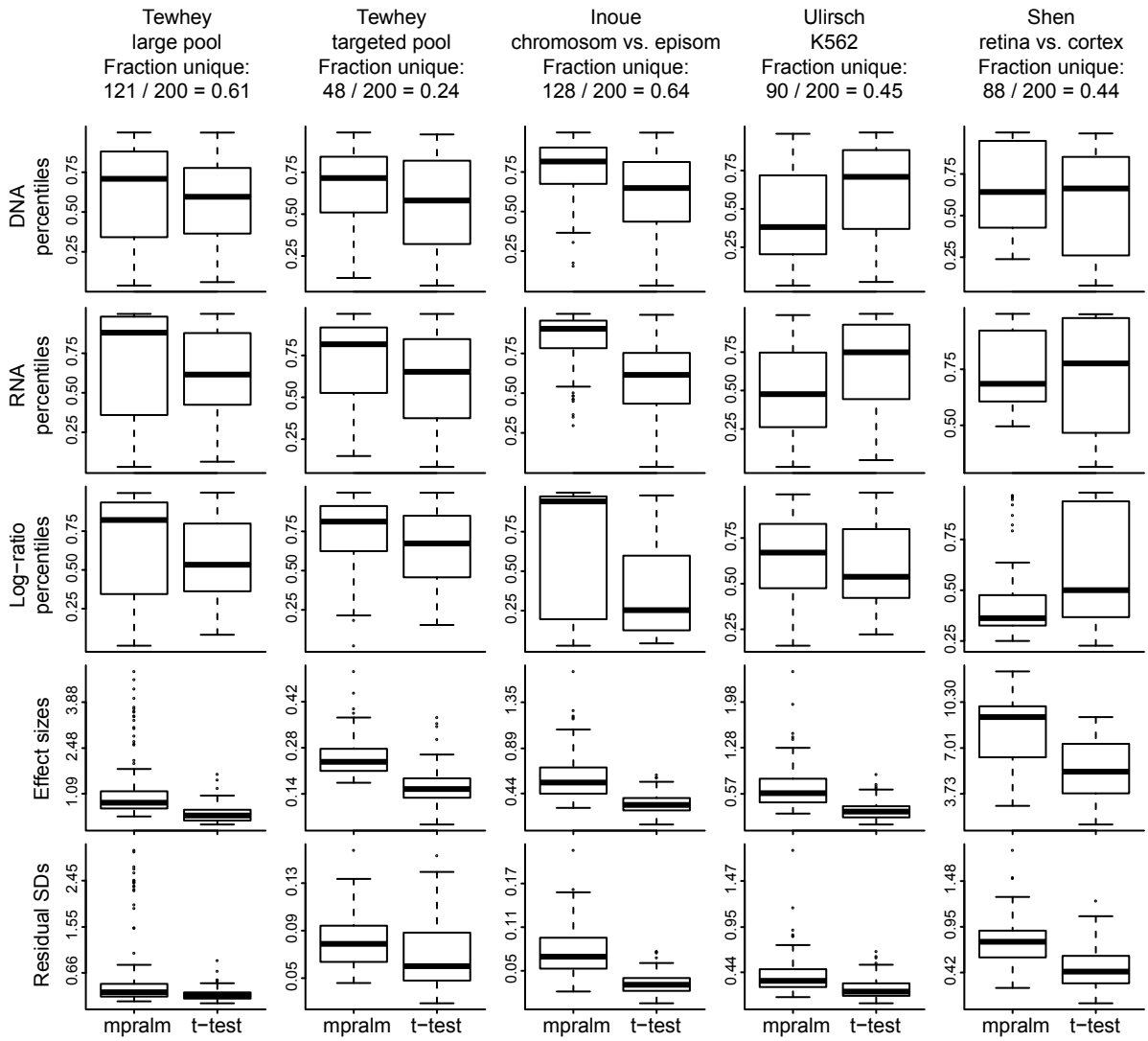

Figure 7. Distribution of quantities related to statistical inference in top ranked elements with mpralm and t-test. MPRA elements that appear in the top 200 elements with one method but not the other are examined here. For these uniquely top ranking elements, the DNA, RNA, and log-ratio percentiles are shown in the first three rows. The effect sizes (difference in mean log-ratios) and residual standard deviations are shown in the last two rows. Overall, uniquely top ranking elements for the t-test tend to have lower log-ratio activity measures, effect sizes, and residual standard deviations.

Accuracy of activity measures and power of differential analysis depends on summarization technique over barcodes

MPRA data initially contain count information at the barcode level, but we typically desire information summarized at the element level for the analysis stage. We examine the

theoretical properties of two summarization methods: averaging and aggregation. Under the assumption that DNA and RNA counts follow a count distribution with a mean-variance relationship, we first show that averaging results in activity estimates with more bias. Second, we show that despite this increased bias, mpralm has higher power with averaging than with aggregation.

Let R_b and D_b denote the RNA and DNA count, respectively, for barcode $b = 1, \ldots, B$ for a putative regulatory element in a given sample. We suppress the dependency of these counts on sample and element. Typically, B is approximately 10 to 15 (for examples, see Table 1). We assume that R_b has mean μ_r and variance $k_r\mu_r$ and that D_b has mean μ_d and variance $k_d\mu_d$. Typically the constants k_d and k_r are greater than 1, modeling overdispersion. Negative binomial models are a particular case with $k = 1 + \phi\mu$, where ϕ is an overdispersion parameter. Also let N_d and N_r indicate the library size for DNA and RNA, respectively, in a given sample. Let p_d and p_r indicate the fraction of reads mapping to element e for DNA and RNA, respectively, in a given sample so that $\mu_r = N_r p_r$ and $\mu_d = N_d p_d$. Let a be the true activity measure for element e defined as $a := \log(p_r/p_d)$. When performing total count normalization, the RNA and DNA counts are typically scaled to a common library size L.

One commonly used estimator of a is an average of barcode-specific log activity measures (which we call the average estimator):

$$\hat{a}^{AV} = \frac{1}{B}\sum_{b=1}^{B} \log\left(\frac{R_b L/N_r + 1}{D_b L/N_d + 1}\right)$$

Using a second order Taylor expansion (Methods), it can be shown that this estimator has bias approximately equal to

$$\text{bias}^{AV} \approx \frac{1}{2}\left(\frac{k_d}{\mu_d} - \frac{k_r}{\mu_r}\right) = \frac{1}{2}\left(\frac{k_d}{N_d p_d} - \frac{k_r}{N_r p_r}\right)$$

Another estimator of a first aggregates counts over barcodes (which we call the aggregate estimator):

$$\hat{a}^{AGG} = \log\left(\frac{1 + (L/N_r)\sum_{b=1}^{B} R_b}{1 + (L/N_d)\sum_{b=1}^{B} D_b}\right)$$

Using an analogous Taylor series argument, we can show that this estimator has bias approximately equal to

$$\text{bias}^{AGG} \approx \frac{1}{B}\text{bias}^{AV}$$

The aggregate estimator has considerably less bias than the average estimator for most MPRA experiments because most experiments use at least 10 barcodes per element. Bias magnitude depends on count levels and the true activity measure a. Further, the direction of bias depends on the relative variability of RNA and DNA counts. Similar Taylor series arguments show that the variance of the two estimators is approximately the same.

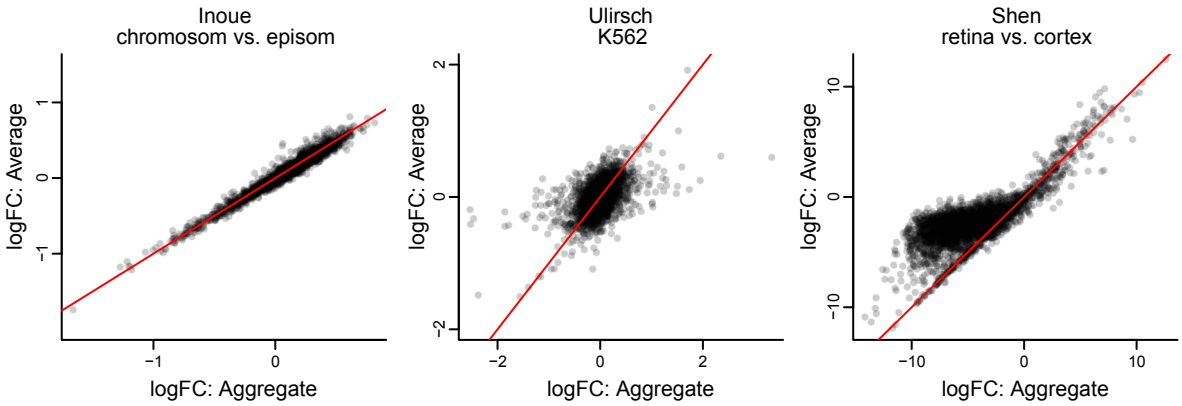

Figure 8. Comparison of the average and aggregate estimators For the three datasets containing barcode-level information, we compare the effect sizes (log fold changes in activity levels) resulting from use of the aggregate and average estimators. The $y = x$ line is shown in red.

The choice of estimator can impact the estimated log fold-changes (changes in activity) in a differential analysis. In Figure 8 we compare the log fold-changes inferred using the two different estimators. For the Inoue dataset, these effect sizes are very similar, but there are larger differences for the Ulirsch and Shen datasets.

The choice of aggregation technique affects power in a differential analysis. In the last three columns of Figures 3, 4, 5, and 6, we compare aggregation to averaging using our mpralm method. Despite the increased bias of the average estimator, it appears to be more powerful than the aggregation estimator. The two estimators have similar type I error rates (Figure 4) but the average estimator results in greater detection rates (Figure 3). We see that when compared at the same observed type I error rates, the average estimator has greater detections (Figure 5). The average estimator also tends to have smaller false discovery rate.

Recommendations for sequencing depth and sample size

To aid in the design of future MPRA experiments, we used the above mathematical model of MPRA to inform power calculations. Power curves are displayed in Figure 9. We observe that the variance of the aggregate estimator depends only minimally on the true unknown activity measure, but is greatly impacted by sequencing depth. Since the impact

of activity measure on variance is minimal, we only need to consider power for a log fold-change (effect size) where we fix one of the two true activity measures to be 0.8. We chose 0.8 as estimated activity measures tend to be around 0.8 in many datasets (Figure 10). We use a nominal type I error rate of 0.05 that has been Bonferroni adjusted for 5000 tests to obtain conservative power estimates. We also use ten barcodes per element as this is typical of many studies.

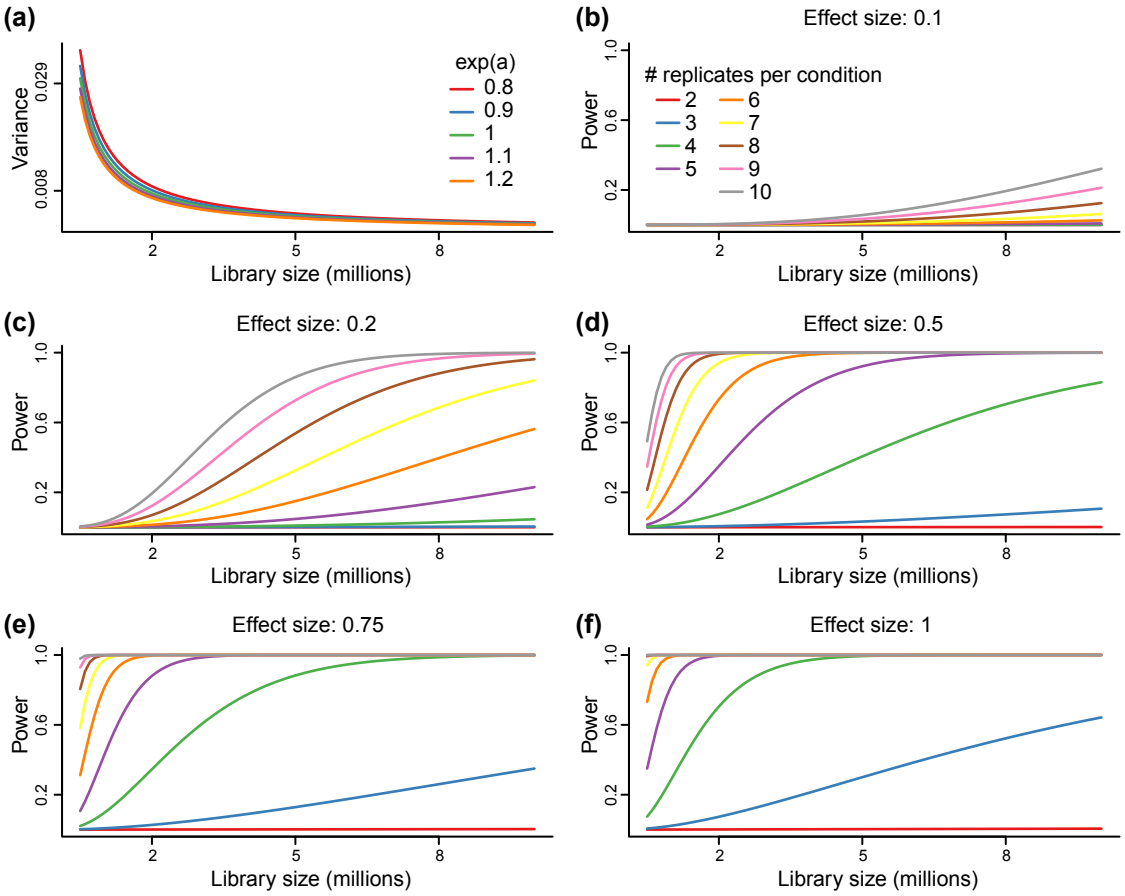

Figure 9. Power analysis. Variance and power calculated based on our theoretical model. **(a)** Variance of the aggregate estimator depends on library size and the true unknown activity level but not considerably on the latter. **(b)-(f)** Power curves as a function of library size for different effect sizes and sample sizes. Effect sizes are $\log_2$ fold-changes.

Our model suggests different impacts of sample size, and a marked impact of increasing the number of replicates, especially between 2 and 6 samples. From Figure 10, we can see that large effect sizes (effect sizes of 1 or greater) are typical for top ranking elements in many MPRA studies. Our model suggests that in this situation it is advisable to do 4 or more replicates per group.

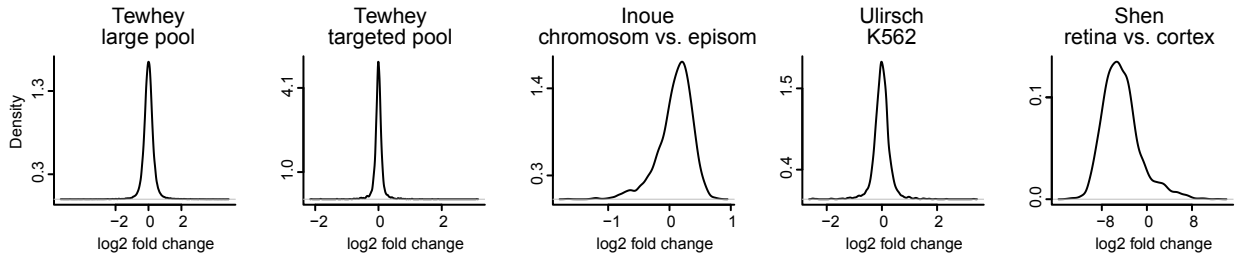

Figure 10. Effect size distributions across datasets. Effect sizes in MPRA differential analysis are the (precision-weighted) differences in activity scores between groups, also called $\log_2$ fold-changes. The distribution of $\log_2$ fold changes resulting from using mpralm with the aggregate estimator are shown here.

Discussion

The field of MPRA data analysis has been fragmented and consists of a large collection of study-specific ad-hoc methods. Our objective in this work has been to provide a unified framework for the analysis of MPRA data. We have pursued this on two fronts. First, we have investigated techniques for summarizing information over barcodes. Second, we have developed a linear model framework, mpralm, for powerful and well-calibrated differential analysis. Third, we have analyzed the impact of sequencing depth and number of replicates on power.

The activity of a regulatory element can be quantified with the log ratio of RNA counts to DNA counts. In the literature, groups have generally taken two approaches to summarizing barcode information to obtain one such activity measure per element per sample. One approach is to add RNA and DNA counts from all barcodes to effectively increase sequencing depth for an element. This is termed the aggregate estimator. Another approach is to compute the log ratio measure for each barcode and use an average of these measures as the activity score for an element. This is termed the average estimator, and we have shown that although it is more biased than the aggregate estimator, it seems to lead to greater power in differential analysis. However, because of this bias, we do caution against the use of the average estimator when comparing activity scores in enhancer groups (often defined by sequence features).

In addition to barcode summarization recommendations, we have proposed a linear model framework, mpralm, for the differential analysis of MPRA data. Our evaluations show that it is well calibrated in terms of type I error rates and p-value distributions. We also see that it is as or more powerful that existing methods being used in the literature. In particular, it seems to be more powerful than existing methods in terms of false discovery rate for top ranking elements, which are quite often the ones prioritized for more intensive follow-up experimentation.

Surprisingly, in our evaluations, t-tests perform well. We caution that this performance depends on addressing their poorly calibrated error rates using permutations. Doing this is critical to obtaining useful results for this method.

Linear models come with analytic flexibility that is necessary to handle diverse MPRA designs. Paired designs involving alleles, for example, are easily handled with linear mixed effects models due to computational tractability. The studies we have analyzed here only consider two alleles per locus. It is possible to have more than two alleles at a locus, and such a situation cannot be addressed with paired t-tests, but is easily analyzed using mpralm. This is important because we believe such studies will eventually become routine for understanding results from genome-wide association studies.

While we have focused on characterizing the mpralm linear model framework for differential analysis, it is possible to include variance weights in the multi-variate models used in saturation mutagenesis and characterization studies. We expect that modeling the copy number-variance relationship will improve the performance of these models.

For power, we find a substantial impact of increasing the sample size even a little (from 2 to 6 per group). This is an important observation because many MPRA studies use 2 or 3 replicates per group, and our results suggest that power can be substantially increased with even a modest increase in sample size.

In short, the ideas set forth here will aid in making rigorous conclusions from a large variety of future MPRA studies.

Methods

Data

See Table 1. Dataset labels used in figures are accompanied by short descriptions below.

Melnikov: Study of the base-level impact of mutations in two inducible enhancers in humans (Melnikov, Murugan, et al., 2012): a synthetic cAMP-regulated enhancer (CRE) and a virus-inducible interferon-beta enhancer (IFNB). We do not look at the IFNB data because it contains only one sample. We consider 3 datasets: **Melnikov: CRE, single-hit, induced state**: Synthetic cAMP-regulated enhancer, single-hit scanning, induced state. **Melnikov: CRE, multi-hit, uninduced state**: Synthetic cAMP-regulated enhancer, multi-hit sampling, uninduced state. **Melnikov: CRE, multi-hit, induced state**: Synthetic cAMP-regulated enhancer, multi-hit sampling, induced state.

Kheradpour: Study of the base-level impact of mutations in various motifs (Kheradpour et al., 2013). Transfection into HepG2 and K562 cells.

Tewhey: Study of allelic effects in eQTLs (Tewhey et al., 2016). Transfection into two

lymphoblastoid cell lines (NA12878 and NA19239) as well as HepG2. In addition two pools of plasmids are considered: a large screening pool and a smaller, targeted pool, designed based on the results of the large pool. We use data from both the large and the targeted pool in NA12878.

Inoue: chromosomal vs. episomal: Comparison of episomal and chromosomally-integrated constructs (Inoue et al., 2017). This study uses a wild-type and mutant integrase to study the activity of a fixed set of putative regulatory elements in an episomal and a chromosomally-integrated setting, respectively.

Ulirsch: Study of allelic effects in GWAS to understand red blood cell traits (Ulirsch et al., 2016). Transfection into K562 cells as well as K562 with GATA1 overexpressed. We use the data from K562.

Shen: mouse retina vs. cortex: Comparison of cis-regulatory elements in-vivo in mouse retina and cerebral cortex (Shen et al., 2016). Candidate CREs that tile targeted regions are assayed in-vivo in these two mouse tissues with adeno-associated virus delivery.

Count preprocessing

We use total count normalization to account for differences in library size for both DNA and RNA. Specifically, each count in a sample is divided by that sample's library size and scaled so that the library size in all samples is the same. We perform minimal filtering on the counts to remove elements from the analysis that have low counts across all samples. Specifically, we require that DNA counts must be at least 10 in all samples to avoid instability of the log-ratio activity measures. We also remove elements in which these log-ratios are identical across all samples. This is necessary for sensible differential analysis. In practice, log-ratios are only identical across all samples if RNA counts are zero across all samples. Both steps also improve the estimation of the copy number-variance relationship used in subsequent modeling by removing clear outliers.

Estimating the copy number-variance relationship

After preprocessing the first step is to estimate the copy number-variance relationship that will allow for the estimation of element-specific reliability weights. These weights are ultimately used in element-specific weighted regressions. The square root of the standard deviation of the log-ratios over samples are taken as a function of average log DNA levels over samples, and this relationship is fit with a lowess curve. Predicted variances are inverted to form observation-level precision weights.

Modeling

Once the observation-specific weights are calculated, the log-ratios and weights are used in the voom analysis pipeline. If, as in allele-specific activity studies, the different versions of the elements being compared are correlated due to being measured in the same sample, a mixed model is fit for each element using the `duplicateCorrelation` module available within the limma Bioconductor package (Smyth, Michaud, and Scott, 2005).

Running mpralm, QuASAR, t-test, Fisher's exact test

For all methods except for QuASAR, DNA and RNA counts were first corrected for library size with total count normalization. By default, we did not normalize counts before input to QuASAR to accord with sample code provided online and with description provided in the manuscript. These results are shown in this document. We also investigated the impact of performing total count normalization and found nearly identical results (not shown).

For the t-test we computed the aggregate estimator of the log-ratio as the outcome measure.

For Fisher's exact test, we summed DNA and RNA counts in the two conditions to form a 2-by-2 table as input to the procedure.

For QuASAR-MPRA, we summed RNA counts in each condition to get one reference condition count and one alternative condition count per element. We also summed DNA counts in all samples and in the reference condition to get one DNA proportion for each element. These were direct inputs to the method.

Permutation tests

We performed null permutation experiments to estimate empirical type I error rates (denoted by α) at different nominal levels. Specifically, we created permuted sample groups that each were composed half of group 1 samples and half of group 2 samples. For example, in a six versus six comparison, we would select three samples from group 1 and three samples from group 2 to be in the first comparison group. The remaining samples would be in the second comparison group. In this way, we expect no differences in activity measures between the comparison groups. We performed 100 permutations for each dataset if sample sizes permitted. For mpralm only, we mean-centered the log ratio outcomes within comparison groups and permuted the resulting residuals (Jiang, 2017).

Estimation of π_0

The proportion of truly null hypotheses for each dataset was estimated using the "lfdr" method in the `propTrueNull` function within limma (Phipson, 2013). This proportion was estimated for mpralm, t-test, and QuASAR, and the median of these estimates was used as the estimate for π_0 for that dataset. Fisher's exact test was excluded from this estimate because it gave an estimate of π_0 that was considerably smaller than the other methods, and which was dubious in light of its uncontrolled type I error rate. These π_0 estimates are used in the FDR calculations of Figures 6.

Bias and variance of estimators

We use Taylor series arguments to approximate the bias and variance of the aggregate and average estimators. The following summarizes our parametric assumptions:

$$\begin{aligned} \mathrm{E}[R_b] &= \mu_r = N_r p_r & \qquad \mathrm{Var}(R_b) &= k_r \mu_r \\ \mathrm{E}[D_b] &= \mu_d = N_d p_d & \qquad \mathrm{Var}(D_b) &= k_d \mu_d \end{aligned}$$

We suppress the dependency of these parameters on sample and element. Library sizes are given by N. The fraction of reads coming from a given element is given by p. Dispersion parameters are given by k. The common library size resulting from total count normalization is given by L. The true activity measure of a given element is given by $a := \log(p_r/p_d)$.

Average estimator

The "average estimator" of a is an average of barcode-specific log activity measures and is written as:

$$\hat{a}^{AV} = \frac{1}{B} \sum_{b=1}^{B} \log\left(\frac{R_b L/N_r + 1}{D_b L/N_d + 1}\right)$$

The second-order Taylor expansion of the function

$$f(R_b, D_b) = \log(R_b L/N_r + 1) - \log(D_b L/N_d + 1)$$

about the point $(\mathrm{E}[R_b], \mathrm{E}[D_b]) = (\mu_r, \mu_d)$ is:

$$
\begin{aligned}
\log\left(\frac{R_b L/N_r + 1}{D_b L/N_d + 1}\right) \approx \log\left(\mu_r L/N_r + 1\right) - \log\left(\mu_d L/N_d + 1\right) \\
+ (R_b - \mu_r)\frac{L/N_r}{\mu_r L/N_r + 1} - (D_b - \mu_d)\frac{L/N_d}{\mu_d L/N_d + 1} \\
- \frac{(L/N_r)^2}{2(\mu_r L/N_r + 1)^2}(R_b - \mu_r)^2 + \frac{(L/N_d)^2}{2(\mu_d L/N_d + 1)^2}(D_b - \mu_d)^2
\end{aligned}
$$

We use the expansion above to approximate the expectation of the average estimator:

$$
\begin{aligned}
\mathrm{E}\left[\hat{a}^{AV}\right] &\approx \log\left(\frac{\mu_r L/N_r + 1}{\mu_d L/N_d + 1}\right) + \frac{(L/N_d)^2 k_d \mu_d}{2(\mu_d L/N_d + 1)^2} - \frac{(L/N_r)^2 k_r \mu_r}{2(\mu_r L/N_r + 1)^2} \\
&\approx \log\left(\frac{p_r}{p_d}\right) + \frac{k_d}{2\mu_d} - \frac{k_r}{2\mu_r} \\
&= a + \frac{k_d}{2\mu_d} - \frac{k_r}{2\mu_r}
\end{aligned}
$$

We can also approximate the variance under the assumption that the barcode-specific log-ratios are uncorrelated:

$$
\begin{aligned}
\mathrm{Var}(\hat{a}^{AV}) &= \frac{1}{B}\mathrm{Var}\left(\log\left(\frac{R_b L/N_r + 1}{D_b L/N_d + 1}\right)\right) \\
&\approx \frac{(L/N_r)^2 k_r \mu_r}{B(\mu_r L/N_r + 1)^2} + \frac{(L/N_d)^2 k_d \mu_d}{B(\mu_d L/N_d + 1)^2} - \frac{2(L/N_r)(L/N_d)\mathrm{Cov}(R_b, D_b)}{B(\mu_r L/N_r + 1)(\mu_d L/N_d + 1)}
\end{aligned}
$$

Aggregate estimator

The "aggregate estimator" of a first aggregates counts over barcodes and is written as:

$$
\hat{a}^{AGG} = \log\left(\frac{1 + (L/N_r)\sum_{b=1}^{B} R_b}{1 + (L/N_d)\sum_{b=1}^{B} D_b}\right) = \log\left(\frac{1 + (L/N_r)R^{AGG}}{1 + (L/N_d)D^{AGG}}\right)
$$

The second-order Taylor expansion of the function

$$
f(R^{AGG}, D^{AGG}) = \log((L/N_r)R^{AGG} + 1) - \log((L/N_d)D^{AGG} + 1)
$$

about the point $(\mathrm{E}[R^{AGG}], \mathrm{E}[D^{AGG}]) = (B\mu_r, B\mu_d)$ is:

$$
\begin{aligned}
\log\left(\frac{1+(L/N_r)R^{AGG}}{1+(L/N_d)D^{AGG}}\right) &\approx \log\left(B\mu_r L/N_r+1\right)-\log\left(B\mu_d L/N_d+1\right)\\
&+(R^{AGG}-B\mu_r)\frac{L/N_r}{B\mu_r L/N_r+1}-(D^{AGG}-B\mu_d)\frac{L/N_d}{B\mu_d L/N_d+1}\\
&-\frac{(L/N_r)^2}{2(B\mu_r L/N_r+1)^2}(R^{AGG}-B\mu_r)^2+\frac{(L/N_d)^2}{2(B\mu_d L/N_d+1)^2}(D^{AGG}-B\mu_d)^2
\end{aligned}
$$

We use the expansion above to approximate the expectation:

$$
\begin{aligned}
\mathrm{E}\left[\hat{a}^{AGG}\right] &\approx \log\left(\frac{B\mu_r L/N_r+1}{B\mu_d L/N_d+1}\right)+\frac{Bk_d\mu_d(L/N_d)^2}{2(B\mu_d L/N_d+1)^2}-\frac{Bk_r\mu_r(L/N_r)^2}{2(B\mu_r L/N_r+1)^2}\\
&\approx \log\left(\frac{p_r}{p_d}\right)+\frac{k_d}{2B\mu_d}-\frac{k_r}{2B\mu_r}\\
&= a+\frac{k_d}{2B\mu_d}-\frac{k_r}{2B\mu_r}
\end{aligned}
$$

We can also approximate the variance:

$$
\begin{aligned}
&\mathrm{Var}(\hat{a}^{AGG}) \approx\\
&\qquad \frac{(L/N_r)^2Bk_r\mu_r}{(B\mu_r L/N_r+1)^2}+\frac{(L/N_d)^2Bk_d\mu_d}{(B\mu_d L/N_d+1)^2}-\frac{2(L/N_r)(L/N_d)\mathrm{Cov}(R^{AGG},D^{AGG})}{(B\mu_r L/N_r+1)(B\mu_d L/N_d+1)}
\end{aligned}
$$

Acknowledgements

Funding: Research reported in this publication was supported by the National Cancer Institute and the National Institute of General Medical Sciences of the National Institutes of Health under award numbers U24CA180996 and R01GM121459.
Disclaimer: The content is solely the responsibility of the authors and does not necessarily represent the official views of the National Institutes of Health.
Conflict of Interest: None declared.

Bibliography

Birnbaum, R. Y., R. P. Patwardhan, M. J. Kim, G. M. Findlay, B. Martin, J. Zhao, R. J. A. Bell, R. P. Smith, A. A. Ku, J. Shendure, and N. Ahituv (2014). "Systematic dissection of coding exons at single nucleotide resolution supports an additional role in cell-specific transcriptional regulation". *PLOS Genetics* 10, e1004592. DOI: 10.1371/journal.pgen.1004592.

Bullard, J. H., E. Purdom, K. D. Hansen, and S. Dudoit (2010). "Evaluation of statistical methods for normalization and differential expression in mRNA-Seq experiments". *BMC Bioinformatics* 11, p. 94. DOI: 10.1186/1471-2105-11-94.

Dickel, D. E., Y. Zhu, A. S. Nord, J. N. Wylie, J. A. Akiyama, V. Afzal, I. Plajzer-Frick, A. Kirkpatrick, B. Göttgens, B. G. Bruneau, A. Visel, and L. A. Pennacchio (2014). "Function-based identification of mammalian enhancers using site-specific integration". *Nature Methods* 11, pp. 566–571. DOI: 10.1038/nmeth.2886.

Ernst, J., A. Melnikov, X. Zhang, L. Wang, P. Rogov, T. S. Mikkelsen, and M. Kellis (2016). "Genome-scale high-resolution mapping of activating and repressive nucleotides in regulatory regions". *Nature Biotechnology.* 34, pp. 1180–1190. DOI: 10.1038/nbt.3678.

Farley, E. K., K. M. Olson, W. Zhang, A. J. Brandt, D. S. Rokhsar, and M. S. Levine (2015). "Suboptimization of developmental enhancers". *Science* 350, pp. 325–328. DOI: 10.1126/science.aac6948.

Ferreira, L. M. R., T. B. Meissner, T. S. Mikkelsen, W. Mallard, C. W. O'Donnell, T. Tilburgs, H. A. B. Gomes, R. Camahort, R. I. Sherwood, D. K. Gifford, J. L. Rinn, C. A. Cowan, and J. L. Strominger (2016). "A distant trophoblast-specific enhancer controls HLA-G expression at the maternal-fetal interface". *PNAS* 113, pp. 5364–5369. DOI: 10.1073/pnas.1602886113.

Fiore, C. and B. A. Cohen (2016). "Interactions between pluripotency factors specify cis-regulation in embryonic stem cells". *Genome Research* 26, pp. 778–786. DOI: 10.1101/gr.200733.115.

Gisselbrecht, S. S., L. A. Barrera, M. Porsch, A. Aboukhalil, P. W. Estep 3rd, A. Vedenko, A. Palagi, Y. Kim, X. Zhu, B. W. Busser, C. E. Gamble, A. Iagovitina, A. Singhania, A. M. Michelson, and M. L. Bulyk (2013). "Highly parallel assays of tissue-specific enhancers in whole Drosophila embryos". *Nature Methods* 10, pp. 774–780. DOI: 10.1038/nmeth.2558.

Groff, A. F., D. B. Sanchez-Gomez, M. M. L. Soruco, C. Gerhardinger, A. R. Barutcu, E. Li, L. Elcavage, O. Plana, L. V. Sanchez, J. C. Lee, M. Sauvageau, and J. L. Rinn (2016). "In Vivo Characterization of Linc-p21 Reveals Functional cis-Regulatory DNA Elements". *Cell Reports* 16, pp. 2178–2186. DOI: 10.1016/j.celrep.2016.07.050.

Grossman, S. R., X. Zhang, L. Wang, J. Engreitz, A. Melnikov, P. Rogov, R. Tewhey, A. Isakova, B. Deplancke, B. E. Bernstein, T. S. Mikkelsen, and E. S. Lander (2017). "Systematic dissection of genomic features determining transcription factor binding and enhancer function". *PNAS* 114, E1291–E1300. DOI: 10.1073/pnas.1621150114.

Guo, C., I. C. McDowell, M. Nodzenski, D. M. Scholtens, A. S. Allen, W. L. Lowe, and T. E. Reddy (2017). "Transversions have larger regulatory effects than transitions". *BMC Genomics* 18, p. 394. DOI: 10.1186/s12864-017-3785-4.

Inoue, F., M. Kircher, B. Martin, G. M. Cooper, D. M. Witten, M. T. McManus, N. Ahituv, and J. Shendure (2017). "A systematic comparison reveals substantial differences in chromosomal versus episomal encoding of enhancer activity". *Genome Research* 27, pp. 38–52. DOI: 10.1101/gr.212092.116.

Ireland, W. T. and J. B. Kinney (2016). "MPAthic: quantitative modeling of sequence-function relationships for massively parallel assays". *bioRxiv*, p. 054676. DOI: 10.1101/054676.

Jiang, D. (2017). "Adjustment Procedure to Permutation Tests in Epigenomic Differential Analysis". PhD thesis. Johns Hopkins Bloomberg School of Public Health.

Kalita, C. A., G. A. Moyerbrailean, C. Brown, X. Wen, F. Luca, and R. Pique-Regi (2017). "QuASAR-MPRA: Accurate allele-specific analysis for massively parallel reporter assays". *Bioinformatics*. DOI: 10.1093/bioinformatics/btx598.

Kamps-Hughes, N., J. L. Preston, M. A. Randel, and E. A. Johnson (2015). "Genome-wide identification of hypoxia-induced enhancer regions". *PeerJ* 3, e1527. DOI: 10.7717/peerj.1527.

Kheradpour, P., J. Ernst, A. Melnikov, P. Rogov, L. Wang, X. Zhang, J. Alston, T. S. Mikkelsen, and M. Kellis (2013). "Systematic dissection of regulatory motifs in 2000 predicted human enhancers using a massively parallel reporter assay". *Genome Research* 23, pp. 800–811. DOI: 10.1101/gr.144899.112.

Kwasnieski, J. C., C. Fiore, H. G. Chaudhari, and B. A. Cohen (2014). "High-throughput functional testing of ENCODE segmentation predictions". *Genome Research* 24, pp. 1595–1602. DOI: 10.1101/gr.173518.114.

Kwasnieski, J. C., I. Mogno, C. A. Myers, J. C. Corbo, and B. A. Cohen (2012). "Complex effects of nucleotide variants in a mammalian cis-regulatory element". *PNAS* 109, pp. 19498–19503. DOI: 10.1073/pnas.1210678109.

Law, C. W., Y. Chen, W. Shi, and G. K. Smyth (2014). "voom: Precision weights unlock linear model analysis tools for RNA-seq read counts". *Genome Biology* 15, R29. DOI: 10.1186/gb-2014-15-2-r29.

Levo, M., T. Avnit-Sagi, M. Lotan-Pompan, Y. Kalma, A. Weinberger, Z. Yakhini, and E. Segal (2017). "Systematic Investigation of Transcription Factor Activity in the Context of Chromatin Using Massively Parallel Binding and Expression Assays". *Mol. Cell* 65, 604–617.e6. DOI: 10.1016/j.molcel.2017.01.007.

Love, M. I., W. Huber, and S. Anders (2014). "Moderated estimation of fold change and dispersion for RNA-seq data with DESeq2". *Genome Biology* 15, p. 550. DOI: 10.1186/s13059-014-0550-8.

Maricque, B. B., J. Dougherty, and B. A. Cohen (2017). "A genome-integrated massively parallel reporter assay reveals DNA sequence determinants of cis-regulatory activity in neural cells". *Nucleic Acids Research* 45, e16–e16. DOI: 10.1093/nar/gkw942.

Marioni, J. C., C. E. Mason, S. M. Mane, M. Stephens, and Y. Gilad (2008). "RNA-seq: an assessment of technical reproducibility and comparison with gene expression arrays". *Genome Research* 18, pp. 1509–1517. DOI: 10.1101/gr.079558.108.

McCarthy, D. J., Y. Chen, and G. K. Smyth (2012). "Differential expression analysis of multifactor RNA-Seq experiments with respect to biological variation". *Nucleic Acids Research* 40, pp. 4288–4297. DOI: 10.1093/nar/gks042.

Melnikov, A., A. Murugan, X. Zhang, T. Tesileanu, L. Wang, P. Rogov, S. Feizi, A. Gnirke, C. G. Callan Jr, J. B. Kinney, M. Kellis, E. S. Lander, and T. S. Mikkelsen (2012). "Systematic dissection and optimization of inducible enhancers in human cells using a massively parallel reporter assay". *Nature Biotechnology* 30, pp. 271–277. DOI: 10.1038/nbt.2137.

Melnikov, A., X. Zhang, P. Rogov, L. Wang, and T. S. Mikkelsen (2014). "Massively parallel reporter assays in cultured mammalian cells". *J. Vis. Exp.* DOI: 10.3791/51719.

Mogno, I., J. C. Kwasnieski, and B. A. Cohen (2013). "Massively parallel synthetic promoter assays reveal the in vivo effects of binding site variants". *Genome Research* 23, pp. 1908–1915. DOI: 10.1101/gr.157891.113.

Patwardhan, R. P., J. B. Hiatt, D. M. Witten, M. J. Kim, R. P. Smith, D. May, C. Lee, J. M. Andrie, S.-I. Lee, G. M. Cooper, N. Ahituv, L. A. Pennacchio, and J. Shendure (2012). "Massively parallel functional dissection of mammalian enhancers in vivo". *Nature Biotechnology* 30, pp. 265–270. DOI: 10.1038/nbt.2136.

Patwardhan, R. P., C. Lee, O. Litvin, D. L. Young, D. Pe'er, and J. Shendure (2009). "High-resolution analysis of DNA regulatory elements by synthetic saturation mutagenesis". *Nature Biotechnology* 27, pp. 1173–1175. DOI: 10.1038/nbt.1589.

Phipson, B. (2013). "Empirical bayes modelling of expression profiles and their associations". PhD thesis.

Robinson, M. D., D. J. McCarthy, and G. K. Smyth (2010). "edgeR: a Bioconductor package for differential expression analysis of digital gene expression data". *Bioinformatics* 26, pp. 139–140. DOI: 10.1093/bioinformatics/btp616.

Safra, M., R. Nir, D. Farouq, I. Vainberg Slutskin, and S. Schwartz (2017). "TRUB1 is the predominant pseudouridine synthase acting on mammalian mRNA via a predictable and conserved code". *Genome Research* 27, pp. 393–406. DOI: 10.1101/gr.207613.116.

Shen, S. Q., C. A. Myers, A. E. O. Hughes, L. C. Byrne, J. G. Flannery, and J. C. Corbo (2016). "Massively parallel cis-regulatory analysis in the mammalian central nervous system". *Genome Research* 26, pp. 238–255. DOI: 10.1101/gr.193789.115.

Smith, R. P., L. Taher, R. P. Patwardhan, M. J. Kim, F. Inoue, J. Shendure, I. Ovcharenko, and N. Ahituv (2013). "Massively parallel decoding of mammalian regulatory sequences supports a flexible organizational model". *Nature Genetics* 45, pp. 1021–1028. DOI: 10.1038/ng.2713.

Smyth, G. K., J. Michaud, and H. S. Scott (2005). "Use of within-array replicate spots for assessing differential expression in microarray experiments". *Bioinformatics* 21, pp. 2067–2075. DOI: 10.1093/bioinformatics/bti270.

Tewhey, R., D. Kotliar, D. S. Park, B. Liu, S. Winnicki, S. K. Reilly, K. G. Andersen, T. S. Mikkelsen, E. S. Lander, S. F. Schaffner, and P. C. Sabeti (2016). "Direct Identification of Hundreds of Expression-Modulating Variants using a Multiplexed Reporter Assay". *Cell* 165.6, pp. 1519–1529. DOI: 10.1016/j.cell.2016.04.027.

Ulirsch, J. C., S. K. Nandakumar, L. Wang, F. C. Giani, X. Zhang, P. Rogov, A. Melnikov, P. McDonel, R. Do, T. S. Mikkelsen, and V. G. Sankaran (2016). "Systematic Functional Dissection of Common Genetic Variation Affecting Red Blood Cell Traits". *Cell* 165, pp. 1530–1545. DOI: 10.1016/j.cell.2016.04.048.

Vockley, C. M., C. Guo, W. H. Majoros, M. Nodzenski, D. M. Scholtens, M. G. Hayes, W. L. Lowe Jr, and T. E. Reddy (2015). "Massively parallel quantification of the regulatory effects of noncoding genetic variation in a human cohort". *Genome Research* 25, pp. 1206–1214. DOI: 10.1101/gr.190090.115.

White, M. A. (2015). "Understanding how cis-regulatory function is encoded in DNA sequence using massively parallel reporter assays and designed sequences". *Genomics* 106, pp. 165–170. DOI: 10.1016/j.ygeno.2015.06.003.

White, M. A., J. C. Kwasnieski, C. A. Myers, S. Q. Shen, J. C. Corbo, and B. A. Cohen (2016). "A Simple Grammar Defines Activating and Repressing cis-Regulatory Elements in Photoreceptors". *Cell Reports* 5, pp. 1247–1254. DOI: 10.1016/j.celrep.2016.09.066.

White, M. A., C. A. Myers, J. C. Corbo, and B. A. Cohen (2013). "Massively parallel in vivo enhancer assay reveals that highly local features determine the cis-regulatory function of ChIP-seq peaks". *PNAS* 110.29, pp. 11952–11957. DOI: 10.1073/pnas.1307449110.

Zhao, W., J. L. Pollack, D. P. Blagev, N. Zaitlen, M. T. McManus, and D. J. Erle (2014). "Massively parallel functional annotation of 3′ untranslated regions". *Nature Biotechnology* 32, pp. 387–391. DOI: 10.1038/nbt.2851.